AD 777 653

AD-777 653

SILVER/SILVER CHLORIDE ELECTRODE: CHARGING OF A POROUS STRUCTURE

S. Szpak, et al

Naval Electronics Laboratory Center
San Diego, California

8 March 1974

UNCLASSIFIED

SECURITY CLASSIFICATION OF THIS PAGE (When Data Entered)

AD-777653

REPORT DOCUMENTATION PAGE

READ INSTRUCTIONS BEFORE COMPLETING FORM

1. REPORT NUMBER: None	2. GOVT ACCESSION NO.
3. RECIPIENT'S CATALOG NUMBER	
4. TITLE (and Subtitle): Silver/Silver Chloride Electrode: Charging of a Porous Structure	5. TYPE OF REPORT & PERIOD COVERED: Final, Jan 1973-July 1973
	6. PERFORMING ORG. REPORT NUMBER
7. AUTHOR(s): S. Szpak, A. Nedoluha, and T. Katan	8. CONTRACT OR GRANT NUMBER(s)
9. PERFORMING ORGANIZATION NAME AND ADDRESS: Naval Electronics Laboratory Center, San Diego, California 92152	10. PROGRAM ELEMENT, PROJECT, TASK AREA & WORK UNIT NUMBERS: Program Element: 61153N; Task Area: RR0240102; Work Unit No. F301
11. CONTROLLING OFFICE NAME AND ADDRESS: Mat. Sci. Div., Office of Naval Research, 800 North Quincy Street, Arlington, Virginia 22217	12. REPORT DATE: 8 March 1974
	13. NUMBER OF PAGES: 45
14. MONITORING AGENCY NAME & ADDRESS (if different from Controlling Office)	15. SECURITY CLASS. (of this report): UNCLASSIFIED
	15a. DECLASSIFICATION/DOWNGRADING SCHEDULE: NA

16. DISTRIBUTION STATEMENT (of this Report)

Approved for public release; distribution is unlimited.

17. DISTRIBUTION STATEMENT (of the abstract entered in Block 20, if different from Report)

18. SUPPLEMENTARY NOTES

Prepared for publication in the Journal of Electrochemical Society

19. KEY WORDS (Continue on reverse side if necessary and identify by block number)

Silver chloride, porous electrode, charge distribution, current distribution, reaction profile.

20. ABSTRACT (Continue on reverse side if necessary and identify by block number)

Reaction profiles for the charging of porous silver electrodes in 1 N KCl are investigated. The effects of changes in the rate determining step on the reaction profile are calculated and compared with experiment for galvanostatically held superficial current densities of 2 to 25 mA/cm^2 for 2 to 8 hours. Interpretations are given for the experimentally determined distributions of anodically formed silver chloride and for the morphology of the silver chloride deposits as observed with the scanning electron microscope as a function of distance into the porous structure.

DD FORM 1 JAN 73 1473 EDITION OF 1 NOV 65 IS OBSOLETE
S/N 0102-014-6601

UNCLASSIFIED
SECURITY CLASSIFICATION OF THIS PAGE (When Data Entered)

SILVER/SILVER CHLORIDE ELECTRODE: CHARGING OF A POROUS STRUCTURE.

S. Szpak and A. Nedoluha
Electronic Materials Sciences Division
Naval Electronics Laboratory Center
San Diego, California 92152
and
T. Katan*
Materials and Structures, Lockheed Palo Alto Research Laboratory,
Palo Alto, California 94304

Abstract

Reaction profiles for the charging of porous silver electrodes in 1 N KCℓ are investigated. The effects of changes in the rate determining step on the reaction profile are calculated and compared with experiment for galvanostatically held superficial current densities of 2 to 25mA/cm^2 for 2 to 8 hours. Interpretations are given for the experimentally determined distributions of anodically formed silver chloride and for the morphology of the silver chloride deposits as observed with the scanning electron microscope as a function of distance into the porous structure.

In recent years several approaches to battery electrode modeling have been proposed. Perhaps the best known and most comprehensive one is that of Bennion and coworkers[1,2] which is based on the solution of a set of coupled partial differential equations representing the various applicable laws of transport and conservation. An effective computer program is available so that, in principle, the reaction profile can be constructed once the details of

---

*Electrochemical Society Active Member

KEYWORDS: Silver chloride, Porous electrode, Charge distribution, Current distribution, Reaction profile.

the reaction mechanism and transport processes within the porous structure have been established.[3] In practice, the difficulty in electrode modeling arises from a lack of sufficiently detailed information concerning the nature of the controlling elementary processes and their dependence on the degree of electrode discharge. Nevertheless, some success has been reported in a comparison of the experimental data of Bro and Kang,[4] with the computer simulated behavior using the solution-diffusion model.[3]

Current experimental efforts in studying the time-dependent evolution of reaction profiles, which are of interest in battery technology, involve the determination of pertinent factors from the analysis of the degree of conversion as a function of distance at externally controlled discharge conditions, e.g., potentiostatic, galvanostatic or an otherwise programmed discharge mode. In general, it is not possible to assign a reaction path on the basis of a chemical analysis of the reaction products as a function of distance alone. Thus, in addition to the usual analytical procedures, Katan[5] and Katan, *et al*[6,7] studied surface morphology after charge and discharge in an attempt to obtain data necessary for modeling the sparingly soluble reactant-conductive matrix system. In an extension of this approach, Bennion and *et al* [8] selected a different geometry to simulate the electrode behavior and employed X-ray element scanning analyses combined with scanning electron microscopy to arrive at the nature of the controlling elementary process.

While electrode modeling can be used to predict electrode behavior and to show very clearly the effects of various elementary processes, modeling per se cannot be used to predict the elementary processes. It is the purpose of this communication to illustrate that a considerable gain into describing

the working of battery electrodes can be achieved using a more restrictive model for which analytical solutions can be given. In particular, we shall consider the situation where the rate determining step changes during the course of electrode discharge. This model is less restrictive than that of Winsel[9] where the reaction path is invariant with time, but certainly is more restrictive than that of Bennion and coworkers.[1,2] The silver/silver chloride electrode will be used here to demonstrate the essential features of this model.

EQUIVALENT CIRCUIT CONCEPT

Elementary model of porous electrode.

An equivalent electric circuit is frequently used to represent behavior of porous electrodes. An extensive review of this concept was given by de Levie.[10] The reaction density profile for a one-dimensional porous electrode of length ℓ, and subject to a galvanostatic mode of operation, i.e., for boundary conditions given by

$$i(o,t) = i_o, \; i(\ell,t) = 0, \tag{1}$$

is as follows:

$$j(x) = \kappa_1 \, i_o \, \frac{\cosh[\kappa_1(\ell-x)]}{\sinh(\kappa_1 \ell)} \, . \tag{2}$$

The transfer (faradaic) current density is given by Eq. (3),

$$j = - \frac{\partial i}{\partial x} \, . \tag{3}$$

The dimensionless parameter $\kappa_1 = (R_1/Z_1)^{\frac{1}{2}}$, is the square root of the ratio of solution resistance to electrode reaction impedance, both per unit length and unit cross section of the porous electrode.

Equation (2) exhibits an exponential behavior; for $j(x) > 0$, the slope $j'(x)$ is negative and its magnitude decreases with an increase in distance. The rate at which $j(x)$ bends away from the x-axis depends on the numerical value of κ_1. This purely geometrical fact can be converted to a useful engineering number. Thus, Winsel[9] refers to it as the reduced pore length, Bro and Kang[4] prefer the name of electrochemical Thiele parameter. Other terms, such as electrode effectiveness factor and depth of penetration, are also associated with it. A formulation by Nanis[11] is especially useful because it reflects the importance of electrode structure as well as the electrochemical process. Regardless of the manner in which this number has been introduced, its use is limited to electrodes under a steady-state regime.

Unfortunately, a true steady state operation cannot be realized in the course of battery discharge, because the supply of reactant is continually diminishing. Corresponding structural changes occur, and when all active material is used up, the electrode ceases to function. The time dependent reaction profile is thus related to the material used up, or, alternatively, to the material still present. It is not surprising, therefore, that the experimentally determined Thiele parameter has been found to vary with the electrode discharge.[4,12]

Porous electrode with change of reaction path.

An electrochemical process, as a rule, consists of a series of consecutive elementary processes. Consequently, there exists a relation

$$Z(x,t) = \Sigma_k Z_k(x,t), \qquad (4)$$

as can be inferred from Van Rysselberghe's analysis of the complex reaction path[13] as indicated by de Levie,[10] and as explicitly derived by Dunning[3] for the "solution-diffusion" model.

Usually one elementary process dominates the overall reaction path, so that the right side of Eq. (4) contains essentially one term. If, in the course of electrode reaction a change in the rate determining step (rds) takes place, only the numerical value of Z is affected, that is to say, again only one term dominates expression (4). A typical example is the reduction of thin films of silver chloride partially covering the silver substrate. It was shown that, as the individual patches of silver chloride become smaller, a change in the rds from chloride diffusion to silver chloride dissolution occurs. [6] If this process is allowed to occur within the confinements of a porous structure, a change in the rds is likely because of the wide variety of local conditions caused by the distribution in transfer current density and the decreased accessibility of electrolyte which effectuates a change in local concentrations.

The extension of an electric circuit analogue concept to include a change in the rds is not difficult to realize. Consider an electroactive substance uniformly dispersed within the conductive porous matrix. Assume that the reaction path is initially governed by one elementary process throughout the electrode thickness. The reaction density profile is described by Eq. (2), with R_1 and Z_1 associated with the assumed reaction path. Due to the non-linear reaction profile, the amount of the active material used up varies with distance. Assume further that, when the amount of active material initially present is reduced to an *a priori* specified level, another reaction path begins to operate. The reaction density profile given by Eq. (2) then no longer applies.

The graphical representation of a change in the rds within the porous electrode is shown in Figure 1. The change from one mechanism to another has occurred at $x = x_c$. To the right, i.e., for $x_c < x \leq \ell$, the initial reaction path operates, while for $0 \leq x < x_c$, another process dominates the electrode discharge.

Obviously, the location at which the change in controlling reaction takes place is determined by the extent of the electrode discharge or charge. It follows that the rational description of electrode operation requires specification of three time intervals, namely, the time before the second mode of electrode operation is initiated, the time during which the first and second modes operate simultaneously, each with its own rds, and the time after the first mode of operation has completely disappeared. The determination of these time intervals, the corresponding reaction profiles, and the velocity at which the plane of change in the rds propagates through the porous structure can be used to constitute the basis for electrode evaluation. The plane at which the change in the rds occurs will henceforth be referred to as the mode interface.

ANALYTICAL FORMULATION

Basic concepts.

Consider a small section of an equivalent electric circuit analogue, shown in Figure 1(b). The current density, $i(x,t)$, and the potential, $u(x,t)$, are related by Eqs. (5) and (6).

$$\frac{\partial u}{\partial x} = - Ri \tag{5}$$

$$\frac{\partial i}{\partial x} = - \frac{u}{Z} \tag{6}$$

The degree of electrode discharge or charge at point , x, and time, t, is given by Eq. (7)

$$M(x,t) = M_o - \alpha Q(x,t). \tag{7}$$

Here, M_o is the initial amount of electroactive material uniformly distributed within the porous structure, α is a proportionality constant, and $Q(x,t)$ is the transferred charge. If the discharge process is initiated at $t = 0$, the charge transferred at time t is given by Eq. (8)

$$Q(x,t) = \int_0^t j(x,t')dt'. \tag{8}$$

We consider $Q(x,t)$ to be always positive and express it in $Asec/cm^3$. When the amount of charge transferred exceeds an *a priori* given amount, that is, when $Q(x,t) > Q_c$, a new reaction path becomes operative, characterized by R_2 and Z_2, as illustrated in Figure 1(a). Thus, the introduction of R_1, Z_1, R_2, and Z_2, identifies two regions within the electrode structure. The region to the left, i.e., for $0 \leq x < x_c$, will be designated as region 2, while the region to the right of the dividing plane at $x = x_c$, will be referred to as region 1.

With the adapted nomenclature, we identify $x_c(t)$ as the position where a change in the rds takes place, for example, from diffusion to dissolution controlled, as illustrated in Figure 1. All relevant quantities pertaining to position $x_c(t)$ will be denoted by subscript c. The quantities of interest in the present communication are: Q_c, the amount of charge transferred, or extent of electrochemical reaction necessary to initiate the change in the rds; $t_c(x)$, the time at which the mode interface arrives at an *a priori* selected position x; $v_c(x)$, the velocity at which the mode interface penetrates the porous structure.

The extent of the electrochemical conversion is defined by Eq. (8); the critical time $t_c(x)$ is the inverse of $x_c(t)$. For j bounded, it follows from Eq. (8) that a critical time, $t_c(0)$, exists such that all of the electrode belongs to region 1 for $t \leq t_c(0)$. Within this time period the electrode operates under one mode, that is to say, the same reaction path operates

throughout the electrode structure. As discharge of the electrode is carried beyond time $t_c(0)$, the mode interface begins to penetrate into the porous structure, reaching the electrode's backside at time $t_c(\ell)$. Thus, at a time greater than $t_c(0)$ but less than $t_c(\ell)$, the electrode operates under two modes, with the change of the rds occurring at position $x_c(t)$.

At times greater than $t_c(\ell)$, the reaction profile is once again controlled by a single mode, i.e., by the new reaction path which supplanted the original one.

The physical significance of $x_c(t)$, and of the charge transferred, Q_c, is clear; practical utilization, however, requires a knowledge of the dependence of these quantities on the nature of electrochemical reaction and the electrode's structure, and information is needed on changes in these dependences which occur during the course of reaction. Specifically, we need the reaction profile at any time, t, the rate of penetration of the mode interface, and the amount of charge transferred. The depth of penetration of the mode interface and the rate of penetration are experimentally accessible[12] without electrode destruction. The reaction profile, on the other hand, is usually not accessible to direct measurement; it is inferred from the changes in chemical composition as a function of time and position. If the reaction profile is known and the model is given, one can compute the corresponding charge transferred; conversely, from experimental information on the extent of the electrode reaction as a function of position and time, the reaction profile can be reconstructed.

Determination of critical time, $t_c(0)$.

From the initiation of electrode discharge at $t = 0$ to the time $t_c(0)$, the reaction profile is given by Eq. (2). The local rate of electrode

reaction, i.e., the transferred faradaic current, $j(x)$, during this period is taken to be independent of time. Hence, it follows from Eq. (7) that

$$Q(x,t) = j(x) \cdot t \tag{9}$$

which, together with Eq. (2), results in

$$t\ (0) = \frac{Q_c}{\kappa_1 i_o} \tanh(\kappa_1 \ell). \tag{10}$$

Evidently, the time necessary for the initiation of a new reaction path is determined by the electrode thickness as well as the initial reaction path. The critical time can be experimentally controlled by the total discharge current density, i_o in Eq. (10).

Transfer current density profile, $j(x,t)$.

The transfer current density distribution representing the reaction rate profile prior to initiation of the new reaction path is given by Eq. (2). A similar expression applies also at times greater than $t_c(\ell)$, except that R_1 and Z_1 are replaced by R_2 and Z_2, denoting the new reaction mechanism.

In this section we will calculate the discharge profiles when the electrode operates with a change of reaction mechanism, that is, discharge profiles for $t_c(0) < t < t_c(\ell)$. The general form for the solution of Eqs. (5) and (6) is given by Eqs. (11) and (12).

$$i = A\, e^{\kappa_2 x} + B\, e^{-\kappa_2 x} \quad \text{for } 0 \le x < x_c\ . \tag{11}$$

$$i = C\, e^{\kappa_1 x} + D\, e^{-\kappa_1 x}\ . \quad \text{for } x_c < x \le \ell\ . \tag{12}$$

Coefficients A, B, C, and D are evaluated using the boundary conditions in Eq. (1) for a galvanostatic discharge together with the condition of continuity for current, i,

and potential, u, at $x = x_c(t)$. After some manipulations, we obtain the coefficients as follows:

$$A = -i_o e^{-\kappa_2 x_c} M^{(-)}/2N \tag{13a}$$

$$B = i_o e^{\kappa_2 x_c} M^{(+)}/2N \tag{13b}$$

$$C = -i_o \zeta_2 e^{-\kappa_1 \ell}/2N \tag{13c}$$

$$D = i_o \zeta_2 e^{\kappa_1 \ell}/2N \tag{13d}$$

where

$$M^{(\pm)} = \zeta_1 \cosh[\kappa_1(\ell - x_c)] \pm \zeta_2 \sinh[\kappa_1(\ell - x_c)] \tag{14}$$

$$N = \zeta_1 \sinh(\kappa_2 x_c) \cosh[\kappa_1(\ell - x_c)] + \zeta_2 \cosh(\kappa_2 x_c) \sinh[\kappa_1(\ell - x_c)], \tag{15}$$

and

$$\zeta_k = (R_k Z_k)^{\frac{1}{2}} \text{ with } k = 1,2.$$

Appropriate substitutions of Eqs. (13) to (15) into Eqs. (11) and (12), followed by differentiation with respect to distance, yield corresponding local current transfer densities;

$$j(x) = \frac{\kappa_2 i_o}{N} \{\zeta_1 \cosh[\kappa_1(\ell - x_c)] \cosh[\kappa_2(x_c - x)] + \zeta_2 \sinh[\kappa_1(\ell - x_c)] \sinh[\kappa_2(x_c - x)]\} \quad \text{for } 0 \leq x < x_c \tag{16}$$

$$j(x) = \frac{\kappa_1 \zeta_2 i_o}{N} \cosh[\kappa_1(\ell - x)] \quad \text{for } x_c < x \leq \ell. \tag{17}$$

Typical current density profiles associated with the change in the reaction path are shown in Figures 2(a), 2(b), and 2(c). They were computed for a selected set of parameters to demonstrate the various types of reaction intensity

profiles that may arise in the course of electrode discharge, or charge. Two typical kinds of interferences affecting the evolution of reaction profile can be distinguished with the derived equations, and they are designated here as choking of the first and second kind. Specifically, Figure 2(a) demonstrates the effect of choking of the first kind where the principal reaction zone, i.e., that portion of the electrode that carries the bulk of the transfer current, is shifted towards the front of the porous structure. This behavior is associated with an increase in electrolyte resistance, either due to depletion by reactive consumption or because of formation of a voluminous precipitate suspended in the electrolyte. Another type of choking, that of the second kind, results in an opposite behavior. An adherent, non-conductive, thin film is formed as a result of the charge transfer, and this causes an increase in reaction impedance. Consequently, there is a shift of the principal reaction zone into the electrode interior, Figure 2(b).

Figure 2(c) illustrates another set of circumstances that may arise, i.e., when the electrode reaction becomes faster as more electroactive substance has been converted. In practice, this may occur upon complexing of the reaction product.

It is seen that the transfer current density profile consists of two regions, with a discontinuity at $x = x_c(t)$. By definition

$$\Delta j_c = \lim_{\varepsilon \to 0} \{j[x_c(t)+\varepsilon, t] - j[x_c(t)-\varepsilon, t]\}, \quad \varepsilon > 0,$$

hence, it follows from Eqs. (16) and (17) that

$$\Delta j_c = (Z_2 - Z_1) \frac{i_o \kappa_2 \kappa_1}{N[x_c(t)]} \cosh[\kappa_1 (2 - x_c(t)] \,. \tag{18}$$

The magnitude of this discontinuity depends on both reaction paths and becomes smaller as the mode interface penetrates deeper into the electrode structure.

Rate of penetration of mode interface, $v_c(x)$.

The determination of the velocity at which the $x_c(t)$ plane penetrates the electrode structure can be used as a tool in the examination of simple models[12] of electrode discharge.

The charge transferred at any point within region 1 is specified by substitution of Eq. (17) into Eq. (8)

$$Q(x,t) = \kappa_1 \zeta_2 i_o \cosh[\kappa_1(\ell-x)] \int_o^t \frac{dt'}{N[x_c(t')]}, \tag{19}$$

but, at $x = x_c(t)$, $Q(x,t) = Q_c$, which is a constant, thus Eq. (19) is an integral equation for $x_c(t)$:

$$\int_o^t \frac{dt'}{N[x_c(t')]} = \frac{Q_c}{\kappa_1 \zeta_2 i_o} \operatorname{sech}[\kappa_1(\ell-x_c(t))]. \tag{20}$$

Upon differentiation of Eq. (20) with respect to t, an expression for the rate of penetration of the mode interface into the porous structure, $v_c(x_c(t)) = dx_c/dt$, can be written as follows:

$$v_c(x) = \frac{i_o}{Q_c} \coth[\kappa_1(\ell-x)] \left\{ \frac{\zeta_1}{\zeta_2} \sinh[\kappa_2 x] + \cosh[\kappa_2 x] \sinh[\kappa_1(\ell-x)] \right\}^{-1}. \tag{21}$$

The functional dependence of v_c on the depth of penetration x_c for a selected group of parameters characteristic of the new reaction path, R_2 and Z_2, is shown in Figure 3. It is seen that, immediately after the initiation of a new reaction path, the velocity of propagation of the mode interface is

calculated by taking the limit of Eq. (21)

$$v_c(o) = \frac{i_o}{Q_c} \coth^2[\kappa_1 \ell] \tag{22}$$

The velocity, v_c, is thus independent of the kinetics of the newly formed reaction.

For penetration of the mode interface to some distance, x_c, which is small enough ($\kappa_2 x_c << 1$) so that $\sinh \kappa_2 x_c \doteq \kappa_2 x_c$, another simplified relationship can be derived:

$$v_c(x) = \frac{i_o}{Q_c} \coth[\kappa_1(\ell - x)] \left\{ \frac{\zeta_1}{Z_2} x + \tanh[\kappa_1(\ell - x)] \right\}^{-1}. \tag{23}$$

The rate of penetration is dependent on the reaction impedance of the new reaction path. Hence, the larger the value of Z_2, the faster the rate of penetration. As Z_2 becomes infinite, as in the case treated by Winsel,[9] Eq. (23) becomes the following:

$$v_c = \frac{i_o}{Q_c} \coth^2[\kappa_1(\ell - x_c)]. \tag{24}$$

Eq. (24) no longer exhibits a minimum in the rate of penetration, as indicated in Figure 3, e.g., curve d.

Charge transfer.

Direct determination of the transfer current density profile in the course of battery electrode operation has not been demonstrated experimentally thus far, although earlier work by Euler[14] has dealt with simulated behavior. Verification of any proposed or assumed mechanism is usually sought via chemical analysis of the electrode interior. Such an approach essentially involves a comparison of the time integral $\int_0^t j(x,t')dt'$, calculated for an assumed

model with the results of chemical analysis. In what follows, we will derive analytical expressions for the charge transferred, i.e., for the extent of reaction, valid for the considered mechanism of two reaction paths operating within the electrode structure at various degrees of electrode discharge.

Consider again Figure 2(b) and select positions within the porous structure as indicated, e.g., $x = a_1$ and $x = a_2$. Transfer current densities at these locations are given by Eqs. (2), (16), and (17) with the extent of reaction obtained from appropriate substitutions into Eq. (8). The integration indicated by Eq. (8) extends over distinct time intervals reflecting the occurrence of significant events within the electrode structure, that is, based on the position where the change in the rds takes place.

The first time interval, characteristic of the assumed model, is the time before the onset of the new reaction path. This time has been denoted by $t_c(0)$. The integration indicated by Eq. (8) is particularly simple because the reaction profile is time independent. Hence,

$$Q(a_1,t) = i_o \kappa_1 \frac{\cosh[\kappa_1(\ell-a_1]}{\sinh(\kappa_1 \ell]} t \qquad (25)$$

which, at $t = t_c(0)$, becomes

$$Q[a_1,t_c(0)] = Q_c \frac{\cosh[\kappa_1(\ell-a_1)]}{\cosh(\kappa_1 \ell)} . \qquad (26)$$

As the reaction is carried on beyond the critical time, $t_c(0)$, i.e., after the new reaction path is well established, two regions are distinguished. The first region covers depths greater than the position where the change in the rds has taken place, i.e., where $x_c(t) < a_1 \leq \ell$. The second region is concerned with the locations to the left of $x_c(t)$, i.e., for depths less than

determined by the location of the mode interface, that is to say, when $0 \leq a_2 < x_c(t)$.

The charge transferred at any point within region 1 is less than Q_c and is given by Eq. (19). At $x = a_1$ together with Eq. (20), this yields

$$Q(a_1, t) = Q_c \frac{\cosh[\kappa_1(\ell-a_1)]}{\cosh[\kappa_1(\ell-x_c(t))]} . \tag{27}$$

It is seen that the charge transferred depends on the position $x_c(t)$ and only indirectly on the newly generated reaction path.

The calculation of charge transfer in region 2 is performed somewhat differently. The charge accumulated must exceed Q_c (by definition), thus the time integral, Eq. (8), may be split as follows:

$$Q(a_2, t) = Q_c + \int_{t_c(a_2)}^{t} j(a_2, t')dt'. \tag{28}$$

Here, it is convenient to change the integration variable through the use of the expression $v_c(x) = dx_c/dt$, and obtain

$$Q(a_2, t) = Q_c + \int_{a_2}^{x_c(t)} \frac{j[a_2, t_c(x')]}{v_c(x')} dx'. \tag{29}$$

The $j(a_2, t_c(x'))$ and $v_c(x')$, needed in Eq. (29), are given by Eqs. (16) and (21), respectively. Upon substitution we obtain

$$Q(a_2, t) = Q_c \left\{ 1 + \kappa_2 \int_{a_2}^{x_c(t)} \tanh[\kappa_1(\ell-x')] \left\{ \frac{\zeta_1}{\zeta_2} \cosh[\kappa_2(x'-a_2)] + \right. \right. \tag{30}$$

$$\left. \left. + \tanh[\kappa_1(\ell-x'] \sinh[\kappa_2(x'-a_2)] \right\} dx' \right\} .$$

At times greater than $t_c(\ell)$, the electrode once again operates in a single mode of discharge or charge. The expression for the charge transferred is

$$Q(a_2, t) = Q[a_2, t_c(\ell)] + i_o \kappa_2 \frac{\cosh[\kappa_2(\ell - a_2)]}{\sinh[\kappa_2 \ell]} \cdot [t - t_c(\ell)]. \qquad (31)$$

Figure 4 summarizes the behavior of the porous electrode operating with the change in the reaction path when the charge transferred exceeded a given value, Q_c. In particular, curve a is a plot of Eq. (26) at $t = t_c(0)$, i.e., for $x_c = 0$. Curve b illustrates the Q-x relationship at times $t_c(0) < t < t_c(\ell)$, when the electrode experiences a change in the rds at $0 < x_c(t) < \ell$. The (dashed) curve denoted by b', represents the Q-x relationship for the same electrode mechanism, but at some later time. It is seen that the curves are displaced to the right, but are otherwise very similar. The relevant equations are: Eq. (27) for the lower part and Eq. (30) for the upper part. The rate at which the displacement penetrates the electrode structure is, of course, the velocity given by Eq. (21). Finally, curve c_1 illustrates the behavior at time $t \geq t_c(\ell)$, i.e., when the electrode once again operates in a single mode.

COMPARISON WITH EXPERIMENT

Before we proceed with the interpretation of experimental results, it is necessary to review briefly the applied experimental procedures and relate them to the basic assumptions underlying the theoretical development.

The details of the experimental arrangement, including the construction and geometry of the porous electrode employed, were given elsewhere.[5,6] Here, we restrict remarks on experimental procedure to the fact that the porous electrode was constructed by confining loosely packed silver spheres in a glass cylinder and resting the spheres on a silver backing-plate. Such packing assured good electrical conductivity in the electrode matrix, satisfying the assumption of negligibly small ohmic resistance of the matrix in the formulation of the fundamental differential equations, Eqs. (5) and (6). Direct measurements showed that the specific resistance is about 1 Ω cm at the beginning of the charging process, which is indeed negligible when compared with the ohmic resistance of the electrolyte occupying the voids of the porous structure.

For convenience, quantities useful in the interpretation of experimental results pertaining to the porous electrode used in this investigation, are given in Table I.

The Q - x curves.

In accordance with the developed theory, data first obtained by Katan[15] were plotted as the logarithm of the charge transferred, log Q, vs the position within the porous structure, x. The charging current, i_o, and the charging time, t, were used as parameters. The charge transferred, Q, was determined from the amount of silver chloride found within the experimental unit volume. Atomic absorption spectrometry was the analytical technique employed.

A comparison of the experimental plots, shown in Figure 5, with those derived for the assumed model of the electrode operation and displayed in Figure 4, suggests that the silver/silver chloride electrode, on charging appears to exhibit two rds changes rather than one. One would

tend to identify two changes in the rds of the electrode mechanism: One at low surface coverage, corresponding to a coverage of approximately 1%, with Q_c = 1.0 coulomb/experimental unit, and the other at somewhat higher surface coverages associated with passage of about 10 coulombs/experimental unit.

Qualitative agreement with the predicted behavior, nonetheless, is evidenced by displacement of the Q - x curves with change in the charging current, a corollary of Eq. (21) which relates the velocity of penetration of the change in the rds to the charging current. Similar displacement was recorded when the electrode was charged at constant current for various periods of time. Further qualitative agreement is found in the invariance of slopes with the degree of conversion, especially before the critical charge Q_c has been transferred, i.e., at points $x > x_c(t)$. The relevant equations are Eqs. (27) and (30), which indicate that the charge transferred is governed by the location where the change in the reaction mechanism takes place.

Microscopic examination.

In order to determine causes for the aforementioned presence of an additional break in the Q- x curves, located at approximately x = 0.3 cm and independent of the applied charging current, i_o, microscopic examinations of the electrode's interior were undertaken. Representative photographs, showing elements of electrode surface at depths indicated (alongside curve b), Figure 5, are assembled in Figures 6(a) to 6(g).

As one would expect, the electrode surface close to the bulk electrolyte is heavily converted to silver chloride. Nevertheless, the points of contact between the spheres are seen to be preserved, remaining uncoated, so that good electrical conductivity is maintained. The characteristic feature of the front portion of

the electrode is the appearance of a sludge-like, enveloping deposit, resembling in fact, a dried clay. It is noteworthy that the sludge-like deposit is evident until we approach the critical distance, x_c = 0.30cm, and then it abrubtly disappears to be replaced by crystallites. The density of the crystallized conversion product decreases with the electrode depth.

Origin of break in the Q - x curves.

Microscopic examination of the electrode's interior suggests that the porous structure in the proximity of the bulk electrolyte is engaged in processes which are different than those predominant at greater depths.

It is seen in Figure 5, curve b, that the number of coulombs passed through the first experimental unit is approximately 28.0 - a number which exceeds by a factor of 10, the initially available chloride ion content. A similar estimate for x = 0.3cm shows that twice as much chloride was used as was initially present in the pores during the four hours of electrode charging at $i_o = 8.0\ mAcm^{-2}$. Consequently, chloride must be supplied from the bulk electrolyte. An order of magnitude calculation shows that the necessary chloride could have been supplied by diffusional transport alone and that local chloride concentrations in the pores would be quite low. It can be anticipated that significant changes occur in electrolytic conductivity during the course of electrode charging and that some pore blockage takes place, judging the SEM photographs of the series of Figure 6. The consequent increase in electrolytic resistivity would shift the reaction intensity toward the electrode-bulk electrolyte interface, promoting localized surface coverage. The increase in surface coverage by a non-conductive film, however, would tend to force the

transfer current deeper into the electrode structure, thus shifting the region of low chloride content to greater depths. Further shifts are essentially determined by respective interactions of transport and reaction impedances.

The situation just described is shown in Figure 7. It appears that, for $x < a$, the reactive surface within the experimental volume is approaching a condition of full coverage and surface blockage with silver chloride. This would force the transfer current deeper into the electrode structure. Let us further assume that eventually the highest rate of conversion and, consequently, the lowest concentration of available chloride occurs at x=b. Although chloride transport will originate at both sides of x=b, chloride influx will be principally from the bulk electrolyte. Diffusing potassium chloride then comes into contact with deposited silver chloride to form a complex, $AgCl_n^{-(n-1)}$. The complex ions will diffuse along the path indicated in Figure 7. The complex ions diffusing toward the bulk electrolyte are irretrievably lost and are most likely deposited on the counter-electrode. Those ions that diffuse inward will encounter a region deficient in chloride, thus favoring nucleation and crystal growth of AgCl from the liquid phase. This disappearance of the diffusing complex ions sharpens the diffusion front, i.e., increases the concentration gradient, so that there is a rapid termination in diffusing species, and can account for the observed abrupt change in surface morphology at x = 0.3cm, Figure 6(c). Precipitation of AgCl from complex ions releases chloride ions, which further modifies diffusional transport.

On the other hand, the appearance of the second break in the Q - x curve, Figure 5, is consistent with a change in electrochemical reaction path.

Unlike the first break which is attributed solely to transport processes, the second break arises from the interaction of electrochemical processes with transport processes. As will be seen below, the second break can be attributed to depletion of reactant in the electrolyte by electrochemical reaction or to increase in electrolyte ohmic resistivity.

Results tabulated in Table II are in qualitative agreement with the processes shown in Figure 7. The last column of Table II lists the differences in the number of coulombs supplied by the external circuit and that calculated on the basis of chemical analysis. This difference depends on the charging time for a constant charging current and on charging current for a constant charging time in a manner consistent with the loss of silver ions by the mechanism illustrated in Figure 7. It is known that the electrochemical conversion of silver to silver chloride is 100 percent efficient, and the differences therefore are attributed to subsequent dissolution and transport out of the porous structure. For current densities less than $10 mA cm^{-2}$ and times less than 20 minutes, faradaic efficiencies of 100 percent were always maintained in the 1N KCl. In fact, from Table II it is seen that the longer the charging time, the greater the loss. It is noteworthy that the number of coulombs calculated from the extension of the slope shown in Figure 5, from the shaded area, corresponds to within 10 percent to the differences tabulated in Table II. This may be considered as evidence for the correctness of the general assumptions.

Quantitative aspects of electrode charging.

This section is devoted to the quantitative analysis of the experimental curves shown in Figure 5. For this analysis we require, as was shown in

previous sections, the specification of transport and reaction impedances, R_1, R_2, Z_1 and Z_2, and the value of charge transferred, Q_c, associated with the change in reaction path. Of these quantities only one, R_1, can be estimated because the initial concentration of electrolyte is known. In the present work, $R_1 = 14.0$ Ωcm is used. The other impedances are determined from a selection of four points taken from the Q - x curve and from the estimated value of Q_c.

The estimate of the critical charge, Q_c, is not a straightforward procedure. In a semilogarithmic plot of Q vs x, the transferred charge at a sufficient distance above and below x_c is in good approximation represented by straight lines. One might attempt to obtain Q_c as the intersection of the extensions of these straight lines, but this is justified under special conditions only. In region 2, i.e., for $0 \leq x < x_c(t)$, the transferred charge $Q(x,t)$ is given by Eq. (30); in region 1, i.e., for $x_c(t) < x \leq \ell$, the transferred charge obeys Eq. (27). For convenience and without committing a serious error, we assume $\ell \to \infty$ which reduces Eq. (30) to

$$Q_2(x,t) = Q_c + \kappa_2 Q_c \int_x^{x_c(t)} \left\{ \frac{\zeta_1}{\zeta_2} \cosh[\kappa_2(x'-x)] + \sinh[\kappa_2(x'-x)] \right\} dx' \qquad (32)$$

and Eq. (27) to

$$Q_1(x,t) = Q_c e^{\kappa_1[x_c(t) - x]} . \qquad (33)$$

Upon integration, Eq. (32) yields

$$Q_2(x,t) = Q_c + Q_c \left\{ \frac{\zeta_1}{\zeta_2} \sinh[\kappa_2(x'-x)] + \cosh[\kappa_2(x'-x)] \right\}_x^{x_c(t)} . \qquad (34)$$

For $\kappa_2[x_c(t) - x] >> 1$, Eq. (34) takes the form

$$Q_2(x,t) = \frac{1}{2} Q_c \left(\frac{\zeta_1}{\zeta_2} + 1 \right) e^{\kappa_2[x_c(t)-x]} \quad . \tag{35}$$

The asymptotic expressions (33) and (35) intersect at a point x_a with a corresponding charge $Q_1(x_a,t) = Q_2(x_a,t) = Q_a$. We shall designate Q_a as the asymptotic charge. By equating Eqs (33) and (35), we obtain

$$x_c(t) - x_a = \frac{1}{\kappa_1 - \kappa_2} \ln \left[\frac{1}{2} \left(\frac{\zeta_1}{\zeta_2} + 1 \right) \right] \tag{36}$$

Upon substitution of Eq. (36) into Eq. (33), an expression for the relationship between the asymptotic charge Q_a and the critical charge, Q_c, is obtained, namely

$$Q_a = Q_c \left[\frac{1}{2} \left(\frac{\zeta_1}{\zeta_2} + 1 \right) \right]^{\frac{\kappa_1}{\kappa_1 - \kappa_2}} \tag{37}$$

Hence, for finite κ_1 and κ_2, the asymptotic charge Q_a will agree with Q_c only if $R_1 Z_1 = R_2 Z_2$

Evidently, the information contained in the asymptotics of the Q - x curves is insufficient for an unambiguous determination of the critical charge. For this reason, a trial and error procedure was devised, consisting of a selection of "nearly" correct value for Q_c, taken in the vicinity of Q_a (see Figure 5).

In this investigation the following procedure was adapted: Select an arbitrary value for Q_c in the vicinity of Q_a (charge transfer density from

the intercept) and compute the associated electrode parameters: R_2, Z_1 and Z_2; the R_1 is known from the concentration of the dissolved salt. The calculated values are assembled in Table III.

On purely physical grounds we reject those Q_c's which yield R_2 less than R_1 since otherwise we would accept an increase in salt concentration (here potassium chloride) while none can be produced as a result of electrochemical reaction. Also, we reject those Q_c's that yield values higher than 50 ohm. This is equivalent to the statement that the concentration of potassium chloride in region 2 cannot be less than 0.3N. This appears to be a reasonable value in view of the diffusional processes summarized in Figure 7. On this basis alone, a value $0.88 < Q_c < 1.0$ coulomb/exp unit was selected. Further decision is made by inspecting the last column of Table III where the Z_2 values are tabulated. Since the reaction impedance is assumed to be independent of the charging current, we seek such Q_c that the Z_2 values for both charging currents agrees. $Q_c = 0.94$ coulomb/exp unit was selected.

The experimental evaluation of constants: R_1, R_2, Z_1, Z_2 and Q_c are sufficient to describe the electrode behavior. An additional check on correctness of the reported constants can be obtained by comparing the experimentally located $x_c(t)$ with that calculated for a given current density of the charging process.

Upon integration of Eq. (21), we obtain the information sought, i.e., the time necessary for the change in the reaction mechanism to occur at the position $x_c(t)$, namely

$$t_c(x) = t_c(0) + \frac{Q_c}{i_o} \int_o^x \tanh[\kappa_1(\ell-x')] \left\{ \frac{\zeta_1}{\zeta_2} \sinh[\kappa_2 x'] + \cosh[\kappa_2 x'] \tanh[\kappa_1(\ell-x')] \right\} dx'. \tag{38}$$

Note that the Q_c needed in Eq. (38) must be given in coul/cm^3 whereas the values tabulated in Table III used for the determination of electrode process parameters were given per volume of experimental unit, i.e., 0.078cm^3. When the value $Q_c = \frac{.94}{.078} = 12.05$ coul/cm^3, was employed and the integral in Eq. (38) evaluated, $t_c(0.54) = 15700$ sec was obtained. This value compares rather well with the experimental charging time of 14400 sec. The agreement between the experimental value and the calculated value is within 10%.

Reconstructed j(x) curves.

The theoretical transfer current density profile for $R_1 = 14.0$ Ωcm, $R_2 = 33.14$Ωcm, $Z_1 = 1.27$Ωcm^3, $Z_2 = 0.47$Ωcm^3, and $i_o = 8 \times 10^{-3}$ function of position $x_c(t)$ is plotted in Figure 8.

It is seen that for the first 8.0 minutes ($t_c(0) = 452$ sec) the electrode operated with a single reaction path. The current density was exponential within $0 < x < 0.6$cm and starts to flatten out for $x > 0.6$cm. As the new reaction path was established and the electrode operated with a change in the reaction mechanism, most of the current was shifted toward the bulk electrolyte side of the porous structure. Upon initiation of the change in the rds, the contribution in region 1 became insignificant, being less as region 2 was expanding. The velocity of penetration also became less. These two observations appear to be consistent with the surface morphology shown in Figure 6.

One would expect on the basis of reconstructed curves very little difference in surface coverage at depths greater than 0.45cm. Inspection of Figures 6(d) to 6(f) confirms this and indicates that the observed surface coverage in this region was completed within the first eight minutes, i.e., before the new reaction path became operative. Within this time the difference between the current densities is relatively small, $j(0.45) = 6 \times 10^{-2}$ Acm^{-2},

$j(0.9) = 2\times10^{-2}$ Acm^{-2}. It is also seen that irrespective of the location of x_c, most of the current is concentrated near the bulk electrolyte. The small changes in Z_2 are not associated with the surface coverage, but rather they are due to the difference in concentration of $C\ell^-$ ions.

The reconstructed j(x) curves shown in Figure 8 are in agreement with the surface morphology exhibited in Figure 6. It is seen that at depths $x > 0.45cm$ the extent of surface coverage is almost uniform and is developed in the first 8 minutes, i.e., before the new reaction path was established. When the new mechanism became operative, the reaction profile was shifted toward the bulk electrolyte, which for the galvanostatic case, reduced the transfer current density from $j(0.9) = 2.10^{-3}$ to 0.7 mA/cm^3 when the rds reaction front advanced to $x_c = 0.4cm$. Before the change in the rds, the transfer current density was more uniformly distributed throughout the porous structure. For example, when $x_c = 0$, $j(0.4) = 60mAcm^{-3}$ and $j(0.9) = 20mA/cm^3$.

SUMMARY

An analytical method has been formulated to describe the transfer current density in a porous electrode as function of position and time. The mathematical model assumes the electrode mechanism to depend on the amount of the locally transferred charge and accounts for a change in the rate determined step. Application to the silver-silver chloride system and comparison with experiment shows that the depletion of chloride ions initially present in the porous structure is primarily responsible for the location and depth of the principal reaction zone. The performance characteristics of the electrode is further affected by the dissolution of silver chloride and subsequent transport of complex ions. These conclusions were corroborated by examination of the surface morphology.

ACKNOWLEDGEMENT

This work was supported by the Office of Naval Research.

References

1. J. S. Dunning, D. N. Bennion and J. Newman, This Journal, 118, 1251 (1971).
2. J. S. Dunning and D. N. Bennion, Proc. Advances in Battery Technology Symposium, Electrochemical Society, Southern California - Nevada Section, Vol 5, 1972.
3. J. S. Dunning, Ph.D. Thesis, UCLA, 1972.
4. P. Bro and H. Y. Kang, This Journal, 118, 519 (1971).
5. T. Katan, "Electrochemical Characteristics of Porous Silver/Silver Chloride Electrode," Final Report, LMSC - D 309658, 1972
6. T. Katan, S. Szpak and D. N. Bennion, This Journal, 120, 883 (1973).
7. T. Katan, S. Szpak and D. N. Bennion, This Journal, in press.
8. D. N. Bennion, H. Gu, and R. K. Hebbar, "Failure Analysis of Porous Electrodes," UCLA-ENG 7347, May 1973.
9. A. Winsel, Z. Elektrochem., 66, 287 (1962).
10. R. de Levie, "Porous and Rough Electrodes" in Advances in Electrochemistry and Electrochemical Engineering, Vol. 6, Interscience Publ., New York, N.Y. 1966.
11. L. Nanis, Plating, 58, 805 (1971).
12. S. Szpak and G. E. McWilliams, This Journal, 120, 635 (1973).
13. P. Van Rysselberghe, "Some Aspects of the Thermodynamic Structure of Electrochemistry," in Modern Aspects of Electrochemistry, Vol. 4, Plenum Press, New York, 1966.
14. K. J. Euler, Electrochem. Acta, 13, 1533 (1968).

LIST OF SYMBOLS

a - a constant, defined in text.

i - current density (also current in external circuit) in electrolyte, Acm^{-2}.

j = - $\partial i/\partial x$, transfer current (faradaic) density, Acm^{-3}.

k - running index (k=1,2,...).

ℓ - electrode thickness, cm.

M - amount of electroactive material, gcm^{-3}

- a function of x_c, defined by Eq. (14).

N - a function of x_c, defined by Eq. (15).

Q - charge transferred, $Asec/cm^3$.

R - ohmic resistance, Ωcm.

t - time, sec.

u - potential, V.

v - velocity of penetration of rds change, cm/sec,

Z - reaction impedance, Ωcm^3.

x - distance, cm.

GREEK SYMBOLS

α - a proportionality constant, g/Asec.

ε - a small number.

$\kappa_k = (R/Z_k)^{\frac{1}{2}}$, dimensionless parameter.

$\zeta_k = (R_k Z_k)^{\frac{1}{2}}$, resistance, $\Omega^2 cm$.

SUBSCRIPTS: c, a, o, defined in text.

TABLE I.

Summary of Relevant Parameters of Porous Electrode.

Sphere Diameter	$(37.2 \pm 4) \times 10^{-4}$ cm
Weight of Ag per unit	0.49g
Volume of Experimental Unit	$0.078 cm^3$
Volume of Ag per unit	$0.0484 cm^3$
Volume of Electrolyte	$0.030 cm^3$
Surface Area per unit	$76.3 cm^2$
Equivalents of Cl^- ions per unit	2.90 coulombs
Electrolyte	1 N KCl
Cross Section Area	$1.56 cm^2$
Unit Thickness	0.05cm

TABLE II.

Faradaic Losses Upon Charging.

i_o mAcm^{-2}	t, hr	Q_a/exp unit	x_a	% loss
2.0	4.0	1.03	.262	22.59
5.0	4.0	1.22	.478	21.72
8.0	4.0	1.1	.593	23.8
5.0	8.0	1.5	.62	36.0

Q_{ca} charge determined from an intercept, coulombs/experimental unit.

x_{ca} distance determined from intercept, in cm.

TABLE III. EXPERIMENTALLY DETERMINED SUMMARY OF RELEVANT PARAMETERS.

i_o	Q_c	x_c	κ_1	κ_2	ζ_1/ζ_2	R_1	Z_1	R_2	Z_2
5.0×10^{-3}	.75	.54	3.11	10.72	0.071	13.99	1.44	676	5.98
	.80	.518	3.10	10.76	0.24	13.99	1.45	199	1.72
	.88	.48	3.10	10.65	0.61	13.99	1.45	78	0.69
	.92	.46	3.10	10.41	0.88	13.99	1.45	53.3	0.49
	.98	.45	3.10	9.50	1.51	13.99	1.45	28.2	0.31
8.0×10^{-3}	.80	.59	3.31	8.48	0.532	13.99	1.27	67.3	0.93
	.84	.57	3.31	8.45	0.66	13.99	1.27	53.4	0.75
	.88	.56	3.31	8.42	0.80	13.99	1.27	44.13	0.62
	.94	.54	3.31	8.33	1.06	13.99	1.27	33.14	0.47
	1.00	.52	3.31	8.17	1.35	13.99	1.27	25.58	0.38
	1.20	.46	3.31	5.72	4.05	13.99	1.27	5.95	0.181

FIGURE CAPTIONS

Figure 1. Schematic representation of a segment of porous electrode. Upper: change in reaction path at $x=x_c(t)$; initial reaction path at $x>x_c(t)$, newly created path at $x<x_c(t)$. Lower: electric circuit analogue, subscript 1 initial path, 2 reaction path after $Q>Q_c$.

Figure 2. Transfer current density profiles (from Eqs. (16) and (17)) for selected set of parameters: R, Z, and x_c. All curves for $i_o = 5\text{mAcm}^{-2}$ and $\ell = 0.5\text{cm}$.

Figure 2(a). $R_1 = 5$, $Z_1 = Z_2 = 10^{-1}$.

curve a: $x_c = 0$

curve b: $R_2 = 1$, $x_c = 0.125$

curve c: $R_2 = 50$, $x_c = 0.125$

Figure 2(b). $R_1 = 5$, $R_2 = 1$, $Z_1 = 10^{-2}$, and $Z_2 = 10^{-1}$.

curve a: $x_c = 0$

curve b: $x_c = 0.25\text{cm}$

Figure 2(c). $R_1 = R_2 = 5$, $Z_1 = 1$, $Z_2 = 0.1$, $x_c =$

Figure 3. Rate of penetration of the mode interface into the electrode structure as function of reaction impedance

curve a: $Z_1 = 10^{-2}$, $Z_2 = 5.10^{-2}$

curve b: $Z_1 = 10^{-2}$, $Z_2 = 5\text{x}10^{-1}$

curve c: $Z_1 = 10^{-2}$, $Z_2 = 5$

curve d: $Z_1 = 10^{-2}$, $Z_2 = \infty$

$R_1 = R_2 = 5$.

Figure 4. Reaction product distribution at various time or electrode operation

curve a: for $t = t_c(0)$

curve b: for $t_c(0) < t < t_c(\ell)$

curve c: for $t = t_c(\ell)$.

Other data: $i_o = 0.25$ $mAcm^{-2}$, $Q_c = 100.0$

$R_1 = 5.0$ $R_2 = 5.0$

$Z_1 = 10^{-1}$ $Z_2 = 10^{-2}$

Figure 5. A plot of Q vs x as a function of charging current i_o. Curves a, b, and c for i_o = 5, 8, and 25$mAcm^{-2}$, respectively.

Figure 6. Surface morphology at various depths indicated in Figure 5.

Figure 7. Schematic representation of non-electrochemical processes within the porous structure.

Figure 8. Reconstructed j(x) curves for the charging of silver/silver chloride system. $R_1 = 13\,\Omega cm$, $R_2 = 33.1\,\Omega cm$,

$Z_1 = 1.27\Omega cm^3$, $Z_2 = 0.47\Omega cm^3$,

$i_o = 8.0 mA/cm^2$.

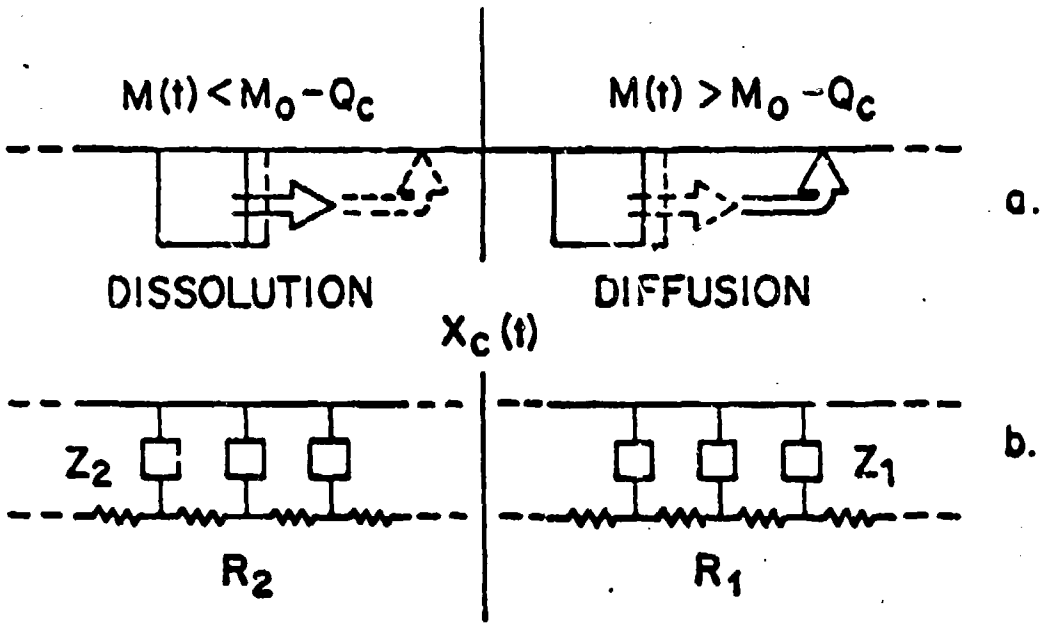

Figure 1

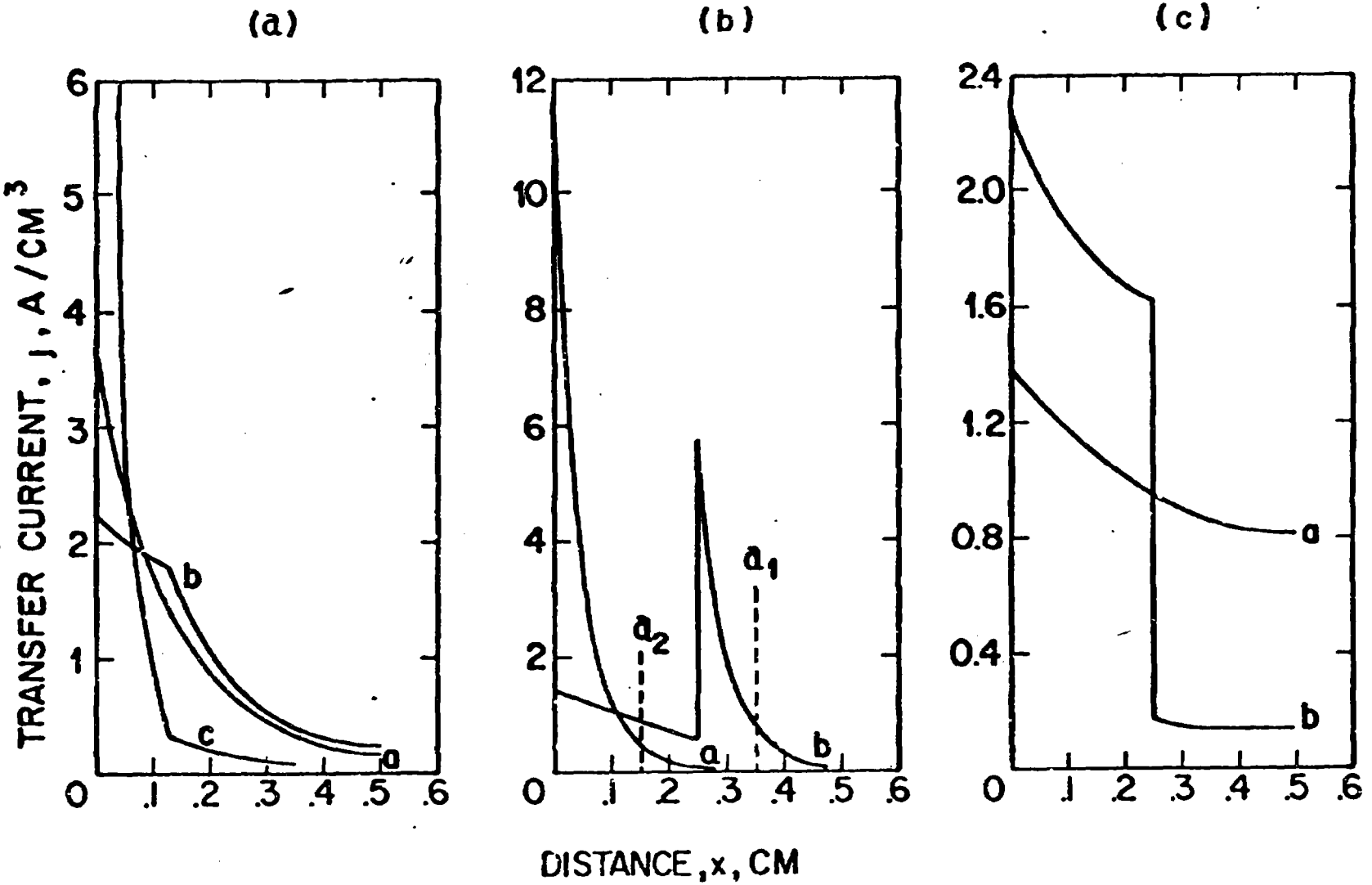

Figure 2

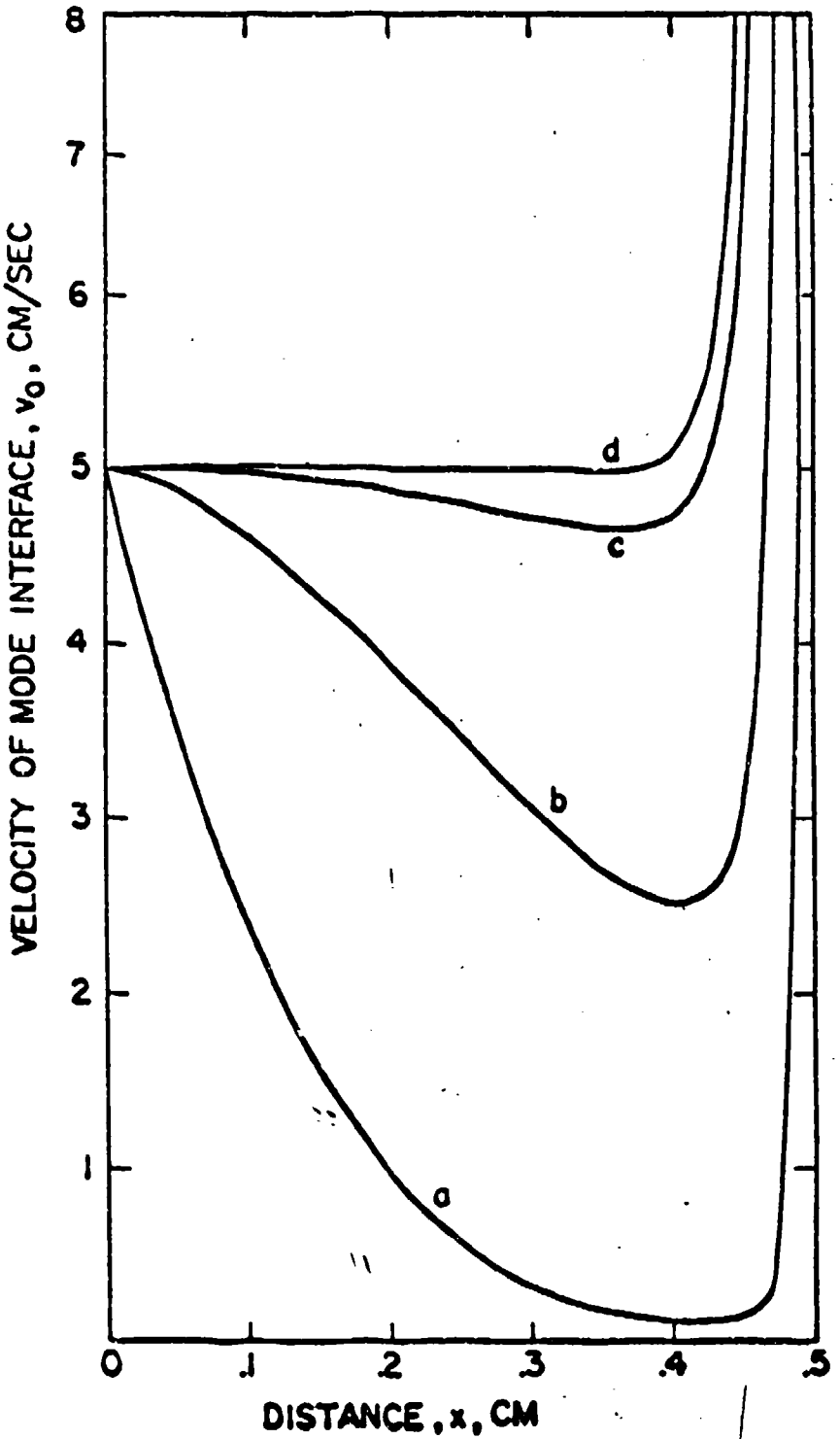
VELOCITY OF MODE INTERFACE, v_0, CM/SEC
DISTANCE, x, CM
8
7
6
5
4
3
2
1
0
.1
.2
.3
.4
.5
a
b
c
d

Figure 3

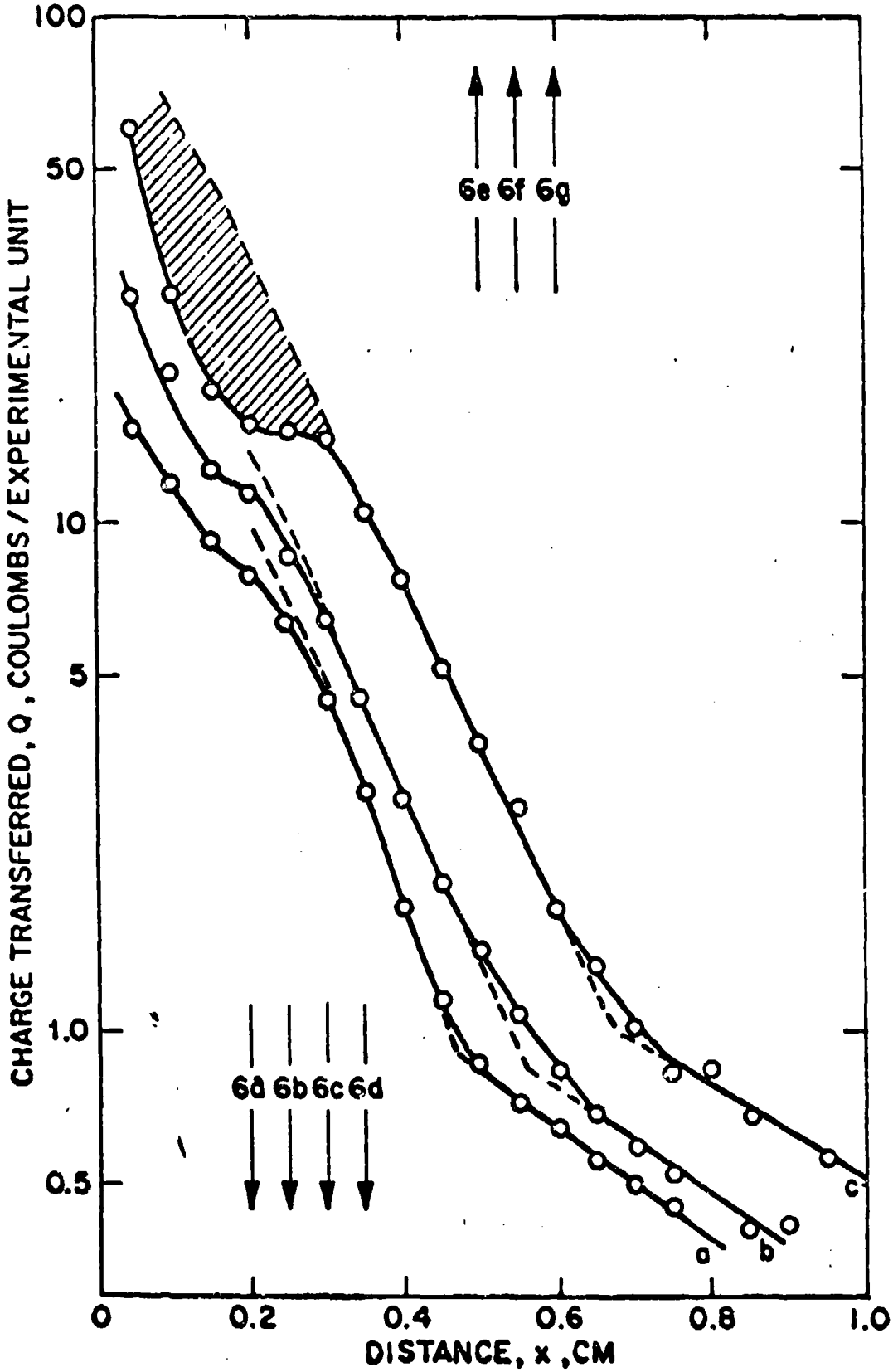
100
50
10
5
1.0
0.5
0
0.2
0.4
0.6
0.8
1.0
CHARGE TRANSFERRED, Q, COULOMBS/EXPERIMENTAL UNIT
DISTANCE, x, CM
6e 6f 6g
6a 6b 6c 6d
a
b
c

Figure 4

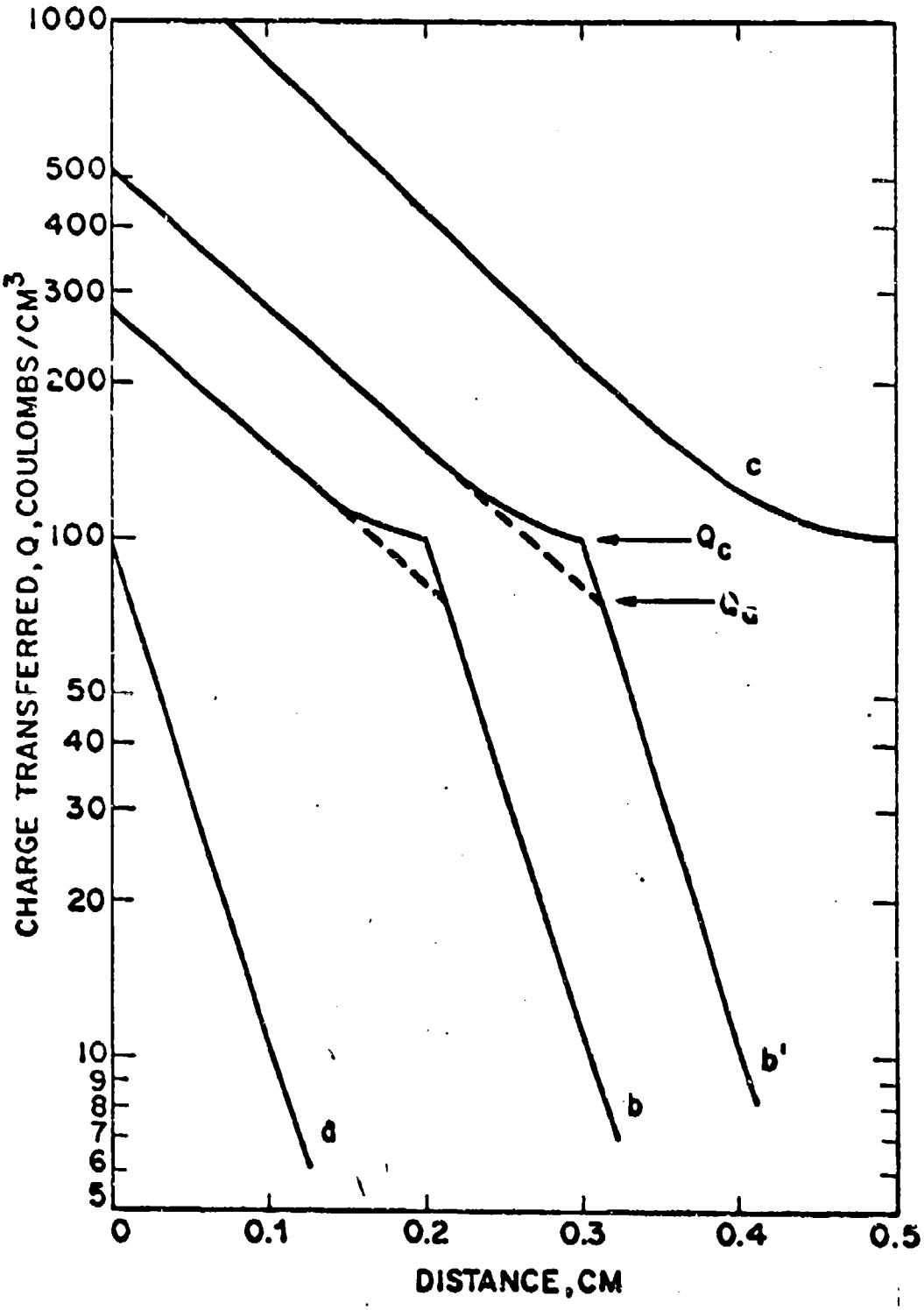
1000
500
400
300
200
100
50
40
30
20
10
9
8
7
6
5
CHARGE TRANSFERRED, Q, COULOMBS/CM³
0
0.1
0.2
0.3
0.4
0.5
DISTANCE, CM
c
Q_c
Q_a
b'
b
a

Figure 5

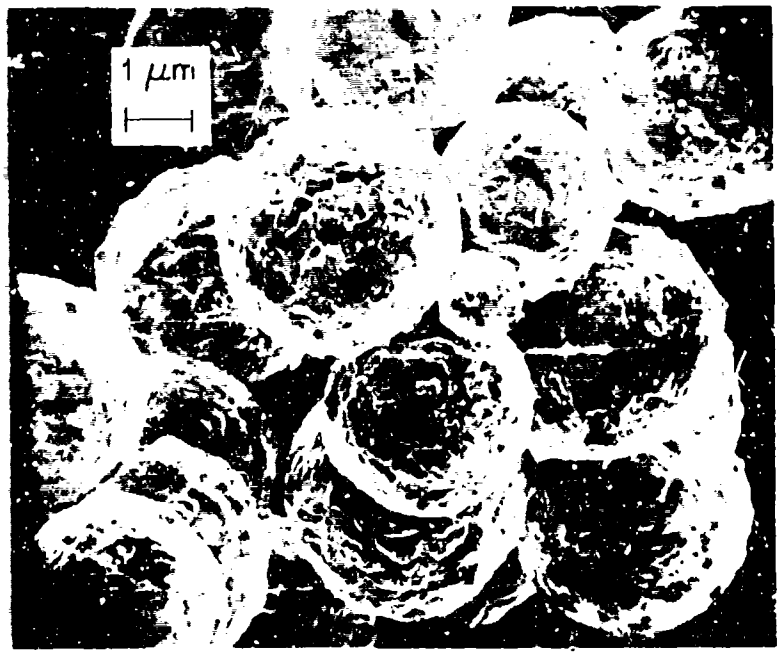
1 μm


1μm

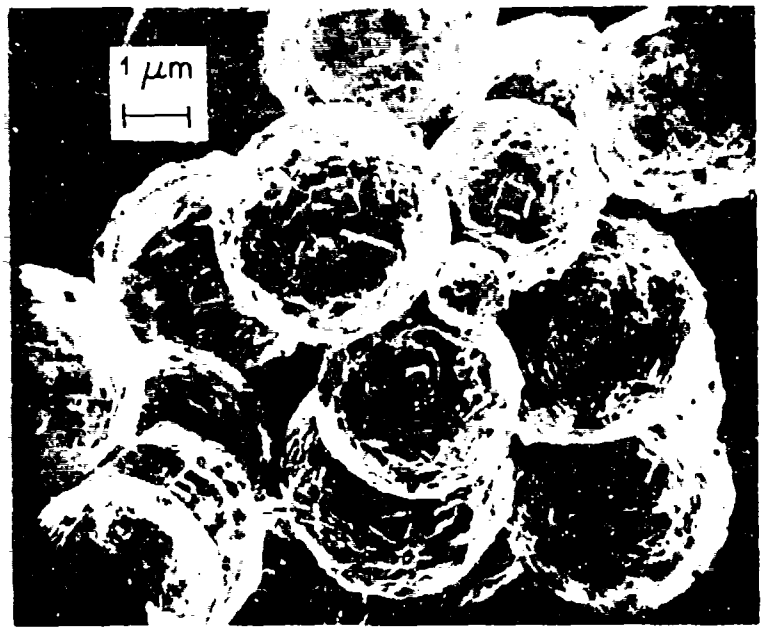

Figure 4a

Figure 4b

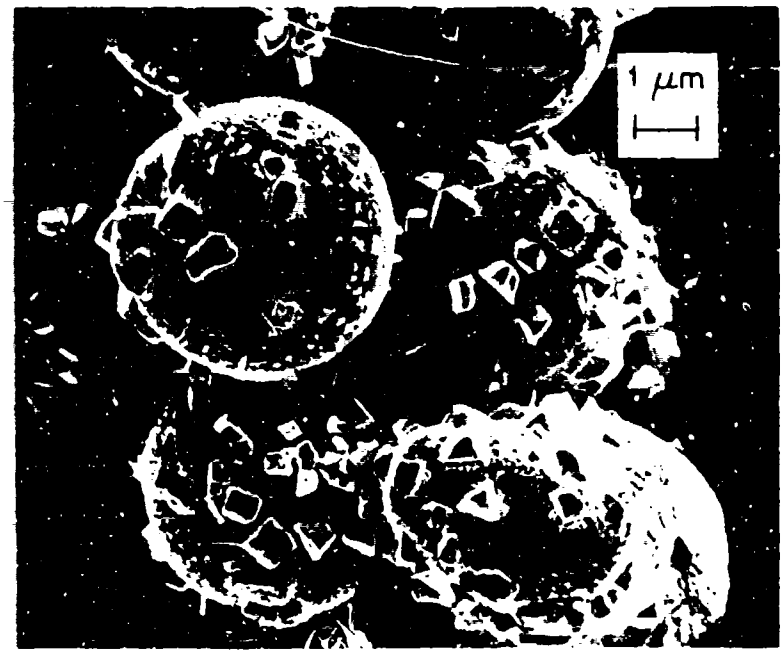
1 μm


1μm

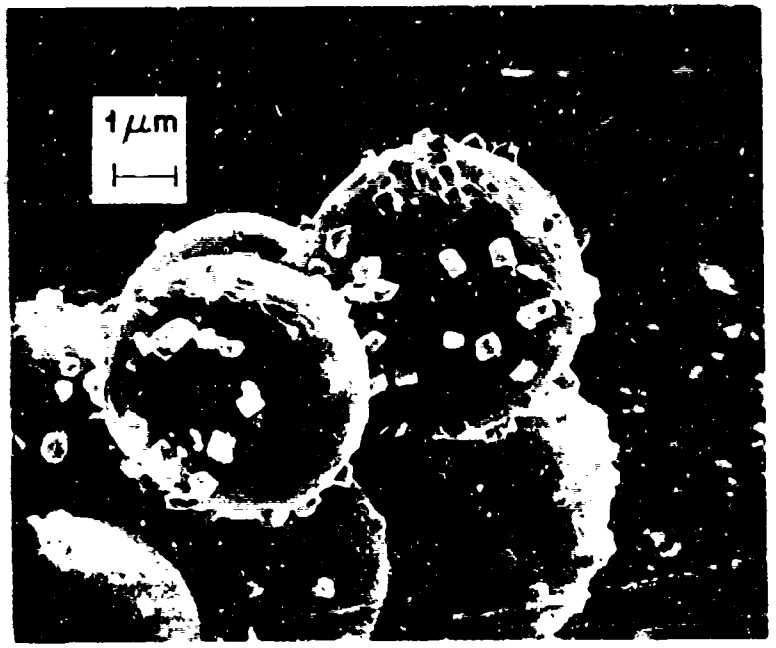
1 μm

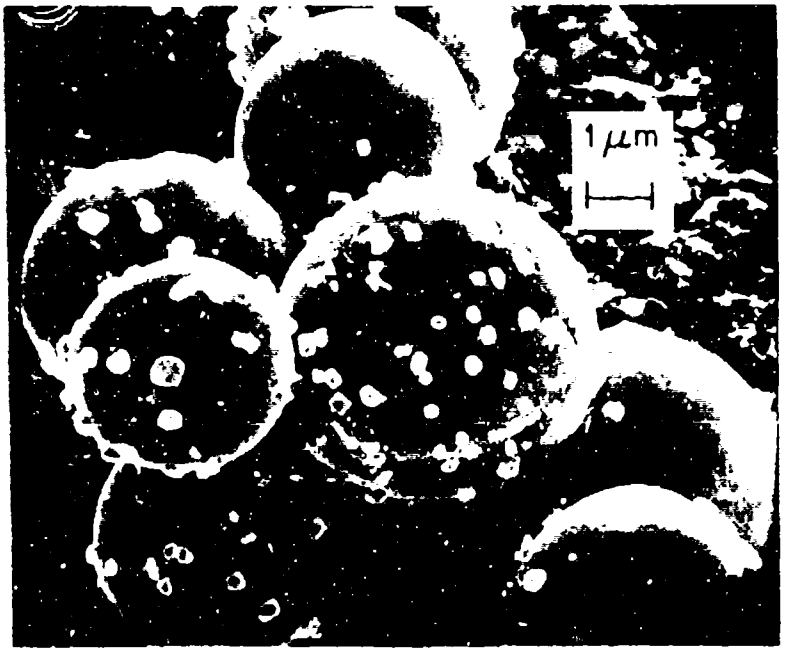
1 μm

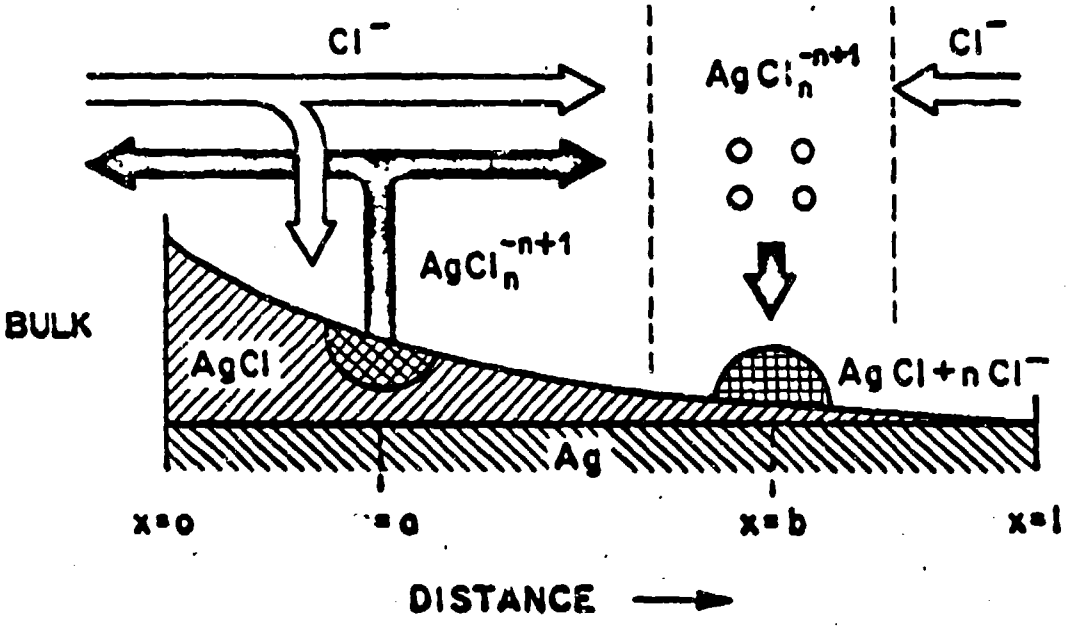
Cl⁻
AgCl$_n^{-n+1}$
Cl⁻
AgCl$_n^{-n+1}$
BULK
AgCl
Ag Cl + n Cl⁻
Ag
x=o
=a
x=b
x=l
DISTANCE

Figure 7

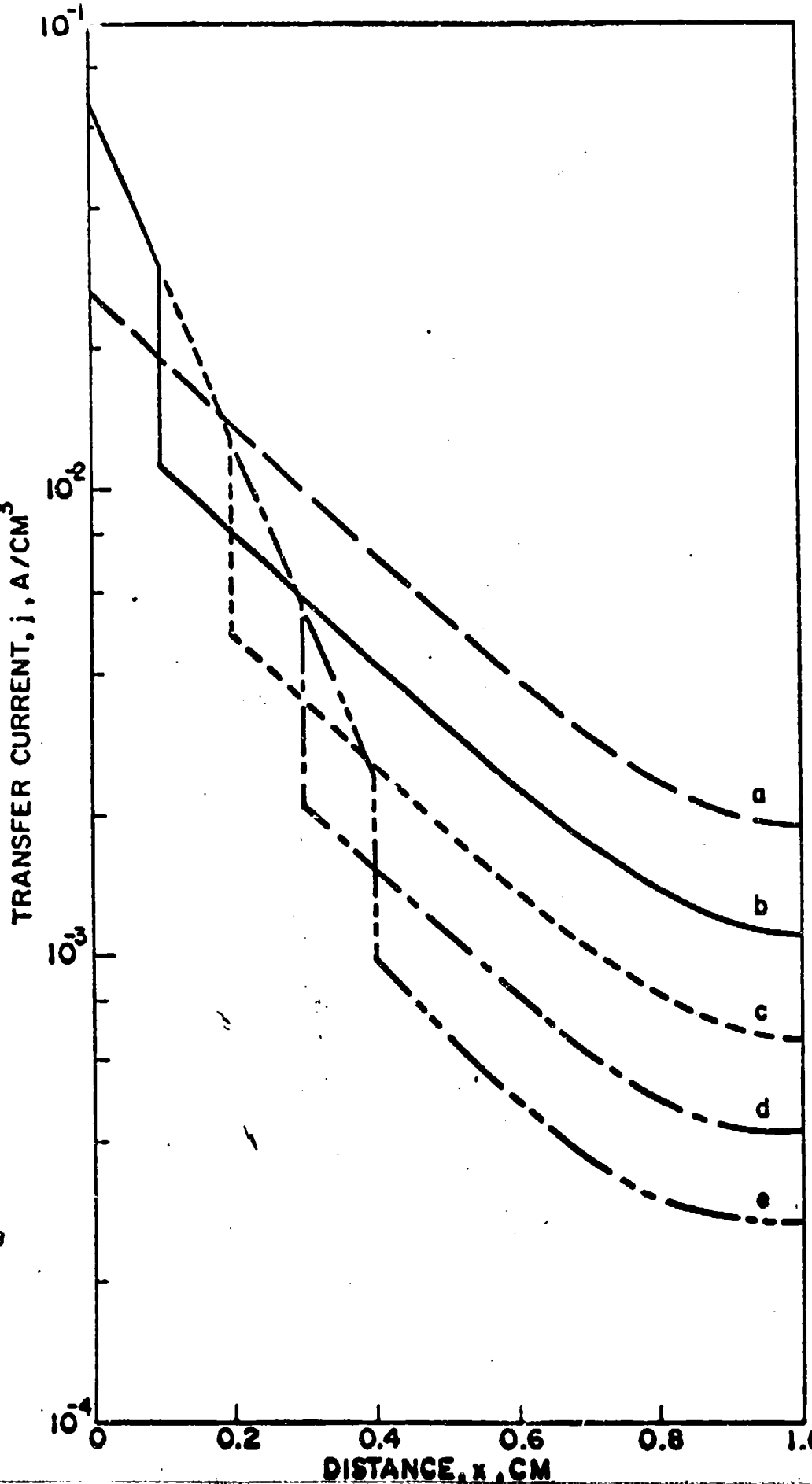
10^{-1}
10^{-2}
10^{-3}
10^{-4}
TRANSFER CURRENT, j, A/CM^3
a
b
c
d
e
0
0.2
0.4
0.6
0.8
1.0
DISTANCE, x, CM

Figure 8